Biomaterials 57 (2015) 22–32

Contents lists available at ScienceDirect

Biomaterials

journal homepage: www.elsevier.com/locate/biomaterials

pH-responsive scaffolds generate a pro-healing response

Jin-Oh You [a, 1, 2], Marjan Rafat [a, 1], Dariela Almeda [a], Natalia Maldonado [b], Peng Guo [a], Christoph S. Nabzdyk [c], Maggie Chun [c], Frank W. LoGerfo [c], John W. Hutchinson [a], Leena K. Pradhan-Nabzdyk [c], Debra T. Auguste [a, d, *]

[a] School of Engineering and Applied Sciences, Harvard University, Cambridge, MA 02138, USA
[b] Department of Biomedical Engineering, City College of New York, New York, NY 10031, USA
[c] Division of Vascular and Endovascular Surgery, Beth Israel Deaconess Medical Center, Boston, MA 02215, USA
[d] Vascular Biology Program, Boston Children's Hospital, Boston, MA 02115, USA

ARTICLE INFO

Article history:
Received 6 January 2015
Received in revised form
2 April 2015
Accepted 3 April 2015
Available online

Keywords:
pH-responsive
DMAEMA
Oxygen transport
Cell infiltration
Tissue engineering

ABSTRACT

A principal challenge in wound healing is a lack of cell recruitment, cell infiltration, and vascularization, which occurs in the absence of temporal and spatial cues. We hypothesized that a scaffold that expands due to local changes in pH may alter oxygen and nutrient transport and the local cell density, leading to enhanced cell deposition and survival. In this study, we present a pH-responsive scaffold that increases oxygen transport, as confirmed by our finite element model analysis, and cell proliferation relative to a non-responsive scaffold. *In vivo*, responsive scaffolds induce a pro-healing gene expression profile indicative of enhanced angiogenesis, granulation tissue formation, and tissue remodeling. Scaffolds that stretch in response to their environment may be a hallmark for tissue regeneration.

1. Introduction

Skin and soft tissue wounds -arising from diabetic foot ulcers, pressure ulcers, and venous ulcers- affect 6.5 million patients in the US at an annual cost of over 25 billion dollars [1]. The pathogenesis is due to a combination of neuropathies, inflammatory irregularities, and peripheral vascular disease. Chronic wounds exhibit increased levels of proteases, impairing remodeling and matrix stability, and hypoxia, impeding immune function and collagen synthesis [2].

The use of skin substitutes provides a structural support that enables cell adhesion, infiltration, and growth [3]. Post-implantation analysis reveals that densely packed, highly metabolic cells (e.g., fibroblasts, endothelial cells, and leukocytes) become paralyzed and apoptotic in the absence of a vascular network, resulting in necrosis [4]. A major contributing factor to this phenomenon is the rapid consumption of diffusing oxygen and nutrients, which limits penetration beyond 100 microns. Efforts to extend cell survival via rapid vascularization led to the fabrication of scaffolds with microfabricated channels [5,6]. These approaches focus on re-engineering the architecture of the scaffold but suffer similar consequences in the absence of anastomosis.

In contrast, stimuli-responsive scaffolds can deform on-demand in response to changes in a cell's environment. Volumetric swelling may be advantageous in wound healing because it convects nutrients when hypoxia is reached and alters the local cell density through the uptake of water. The response is coupled to a decline in pH due to the hydrolysis of ATP and anaerobic glycolysis [7] and an accumulation of metabolic waste [8]. Materials comprised of dimethylaminoethyl methacrylate (DMAEMA), having a pKa of 7.5, swell in response to physiological changes in pH due to the protonation of its tertiary amine [9] Though DMAEMA is extensively used in gene delivery [10,11], its use in tissue engineering is limited.

Herein, we synthesized a series of responsive scaffolds, with varying pH sensitivity, aimed at increasing tissue formation during the early healing period post-implantation. pH-responsive scaffolds exhibited swelling under acidic conditions leading to increased oxygen penetration and cell infiltration, relative to non-responsive scaffolds, which was confirmed by finite element

* Corresponding author. The City College of New York, 160 Convent Avenue T509, New York, NY 10510, USA. Tel.: +1 212 650 7169; fax: +1 212 650 6727.
E-mail address: dauguste@ccny.cuny.edu (D.T. Auguste).
[1] J.-O.Y. and M.R. contributed equally to this work.
[2] Present address: Department of Engineering Chemistry, Chungbuk National University, Cheongju 361-763, Republic of Korea.

http://dx.doi.org/10.1016/j.biomaterials.2015.04.011
0142-9612/

modeling. pH-responsive scaffolds advanced the formation of granulation tissue *in vivo*. The pro-healing response -an increase in growth factors and cytokines that encourage regeneration over inflammation- was induced by scaffolds that can sense and respond mechanically to their environment. pH-responsive scaffolds may provide a platform for the treatment of chronic wounds.

2. Materials and methods

2.1. Synthesis of pH-sensitive scaffolds

600 μL of a poly(methyl methacrylate) (PMMA) microsphere suspension (20 wt%, MW 25k, Thermo Fisher) was placed in a Teflon mold (30 × 10 × 5 mm). After settling, particles were placed at 50 °C overnight for water evaporation and then at 140 °C for 20 h for particle sintering. 200 μL of 2-hydroxyethyl methacrylate (HEMA) and DMAEMA/HEMA solutions (10/90, 20/80, and 30/70, mol/mol; Acros) with 3 mol% tetraethylene glycol dimethacrylate (TEGDMA, Fluka) and 1 mol% 2,2-dimethoxy-2-phenylacet ophoenone (DMPAP, Sigma) were added in the dried PMMA lattice and then placed under UV light (21.7 mW/m^2, 365 nm) for 90 s. After polymerization, gels were immersed in 20 mL of dichloromethane (Mallinckrodt Baker) while shaking vigorously on an orbital shaker for 48 h to remove the PMMA microspheres. The scaffold was placed in 30 mL of diH_2O and washed for 24 h three times. Finally, the scaffold was cut to the desired shape using an 8 mm cork borer.

2.2. Equilibrium swelling studies

Equilibrium swelling of HEMA and DMAEMA/HEMA scaffolds was performed in a 10 mM sodium phosphate buffered medium. The pH was adjusted using 0.1 N HCl to achieve pH 5.5, 6.5, 7.0, and 7.4. Scaffold strips (30 × 10 × 2.0 mm) were placed into a glass jar containing 50 mL of buffer on a shaker (150 ± 1 rpm) at 37 °C. The swelling ratio of the scaffolds as a function of pH was calculated by measuring the mass of the scaffolds at 0, 1, 2, 3, 4, 24, and 48 h by taking the ratio of the swollen scaffold mass over the initial scaffold mass.

2.3. Mechanical testing

The elastic modulus of HEMA and DMAEMA/HEMA scaffolds was measured in 10 mM phosphate buffer at pH 5.5, 6.0, 6.5, 7.0 and 7.4 after fully hydrating for 3 d. Samples were placed on a shaker (150 ± 1 rpm) at 37 °C. Tensile tests of each scaffold strip (30 × 10 × 2.0 mm) were carried out on an Instron BioPuls 5543 using a 500 N loading cell. Scaffolds were strained to failure at a rate of 1 mm/min. The Young's modulus was calculated from the initial 40% strain.

2.4. Cell culture

NIH/3T3 mouse fibroblasts (ATCC# CRL-1658) were cultured at 37 °C in humidified air containing 5% carbon dioxide. NIH/3T3 cells were grown in Dulbecco's Modified Eagle's Medium (DMEM, Life Technologies) supplemented with 10% fetal bovine serum (FBS) and 1% penicillin and streptomycin. Cells were seeded into the scaffolds by dropping 100 μL of cell suspension at either 1.0×10^6 or 1.0×10^7 cells/mL onto dry scaffolds. The cells were incubated for 2 h before adding 1 mL of growth medium to each well and incubating for 5 d.

2.5. Oxygen level and pH change measurements

Oxygen concentration levels in cell-seeded scaffolds (8 × 2 mm) were quantified using OxyLab pO_2 pre-calibrated optical fluorescence probes (Oxford Optronix). HEMA and DMAEMA/HEMA scaffolds were treated with fibronectin (50 μg/mL, pH 7.4) and incubated at room temperature for 1 h in order to allow the extracellular matrix protein to adsorb onto the scaffolds. Scaffolds were seeded with 10^6 or 10^7 NIH/3T3 fibroblasts and maintained in a humidified incubator at 37 °C and 5% CO_2 for 2 h in order to allow for cellular attachment within the scaffold to occur. Oxygen levels were quantified at 0, 24, 48, and 72 h. Measurements were taken in growth media, at the surface and center of the scaffolds for each sample (triplicates for each condition). The oxygen probe was placed at the area of interest until pO_2 readings stabilized. Sensor response time was 5–10 s, which provided a quasi-real time measurement of the oxygen environment. The pH change of growth medium was measured at different incubation times and cell densities using a pH electrode (PHI 255 pH meter, Beckman Coulter).

2.6. Preparation of PLG scaffolds

1 mL of a 10 wt% poly(DL-lactide-co-glycolide) (PLG) solution (50:50 molar ratio, Lactel) in chloroform was mixed with 1.17 g sieved sucrose particles. 200 μL suspensions were placed on a 25 mm concave glass cover and dried in a fume hood for 4 h until all solvent was evaporated. The scaffolds were placed into DI water for 12 h to dissolve the sucrose particles. PLG scaffolds were dried at room temperature for 24 h.

2.7. Cell proliferation under hypoxia

NIH/3T3 cell proliferation on pH-sensitive scaffolds under hypoxia was measured using the Dojindo Cell Counting Kit-8 (Dojindo Molecular Technologies). HEMA, DMAEMA/HEMA, and PLG scaffolds were pre-incubated with 1 mL fibronectin (50 μg/mL, pH 7.4) for 1 h at 37 °C. NIH/3T3 cells were seeded into the scaffolds by dropping 100 μL of cell suspension at 1.0×10^6 cells/mL onto the scaffolds. The cells were incubated at 37 °C under normoxia condition for 2 h. Then 1 mL of growth medium was added to each well, and the scaffolds were incubated under hypoxia (5% O_2, 5% CO_2, balance N_2) for 7 d. Cell viabilities on scaffolds were measured at time points: 1, 3, 5, and 7 d.

2.8. Scanning electron microscopy

Scaffolds containing cells fixed with 2.5% v/v glutaraldehyde in PBS were dehydrated serially in ethanol, critical point dried with liquid CO_2 (Auto Samdri 815 Series A, Tousimis), and sputter coated with Pt/Pd for 2 min at 40 mA (208HR, Cressington Scientific Instruments). Cells were imaged with SEM (FESEM Ultra55, Zeiss) at a beam voltage of 5 kV.

2.9. Oxygen simulation studies

A finite difference mathematical model was developed to predict the oxygen availability in the scaffolds. The 2D model consisted of a scaffold stretching over time increasing its radius from 0.4 cm to 0.72 cm as function of λ(t) (Equation (2)). These scaffold stretch values were obtained experimentally by performing *in vitro* swelling studies. Oxygen outside the scaffold was assumed to be constant. Inside the scaffold a diffusion rate $D = 2 \times 10^{-5}$ cm/s [12], a consumption rate $\beta = 4 \times 10^{-17}$ mol/cell·s [12], an initial cell density $\rho_0 = 10^6$ cells/mL and a scaffold height h = 2 mm were

modeled according to Equations (1) and (3). Results were then compared with non-responsive controls where the radius was kept constant at 0.4 cm or 0.72 cm. Simulation plots were generated using MATLAB®.

2.10. Cell viability

Cell survival after 3 and 6 d was measured using the alamarBlue® fluorometric dye (Life Technologies). 500 μL of fresh growth medium was added to scaffolds. Scaffolds were incubated for 4 h at 37 °C after adding a 50 μL alamarBlue® reagent. Fluorescence was measured at room temperature on a Gemini XPS microplate spectrofluorometer (Molecular Devices) using an excitation of 570 nm and an emission of 585 nm.

2.11. In vivo studies

All animal work was approved by the Beth Israel Deaconess Medical Center's (BIDMC), Institutional Animal Care and Use Committee (IACUC). Wistar rats were obtained from Charles River Laboratories and were between 8 and 12 weeks of age and weighed 350–400 g at the beginning of the study period. 24 Rats were divided into 2 groups for two separate euthanasia time points (7 or 14 d) post-scaffold implantation.

2.12. Animal surgery

Rats were anesthetized using Ketamine (40–80 mg/kg IP) and Xylazine (5–10 mg/kg IP). The dorsal trunk was shaved and the skin was prepped for surgery. Four, 1 cm incisions were made on the dorsum of the rat and a subcutaneous pocket was created. Scaffolds (8 mm × 2 mm) were then inserted inside the subcutaneous compartment in randomized locations. Each rat received a sham subcutaneous pocket (no scaffold), a 100% HEMA scaffold as a control, a DMAEMA/HEMA (30/70, mol/mol) scaffold, and either a DMAEMA/HEMA (20/80 or 10/90, mol/mol) scaffold. Incisions were sutured with 6-0 nylon monofilament suture and the wounds were covered with a triple antibiotic ointment. After surgery, animals were housed in individual cages.

2.13. Tissue harvest

Incisions were made around the subcutaneous pockets and 1 cm^2 sections of skin with the embedded scaffolds were harvested upon euthanasia. Each tissue section was fixed in formalin, divided, and either embedded in paraffin or in OCT and frozen.

2.14. Morphologic analysis and immunohistochemistry (IHC)

Hematoxylin and Eosin (H&E): 6 μm paraffin sections were cut and stained with H&E using standard procedures. CD31 and Neutrophil (CD177): 6 μm OCT embedded frozen sections were fixed with cold acetone for CD31 staining. 6 μm paraffin embedded sections were cut and deparaffinized in xylene and rehydrated. Sections were incubated with Proteinase K solution (Fisher Bioreagents) for antigen retrieval for neutrophil staining. Sections were treated with 3% hydrogen peroxide. Non-serum protein blocking was followed by incubation overnight with primary antibodies (CD31, R&D Systems or CD177, LSbio). Sections were incubated with biotinylated secondary antibodies followed by incubation with the substrate in Nova Red or DAB (Vectastain Mouse Kit; Vectorlabs) and then counterstained with hematoxylin. Macrophages: 6 μm paraffin embedded sections were cut and deparaffinized in xylene and rehydrated. Sections were incubated with Proteinase K solution (Fisher Bioreagents) for antigen retrieval. Standard sequential co-staining methodology was used. Mouse anti rat CD-68 antibody (AbD Serotec) was used to stain all macrophages, anti-TNFα/TNF (LSbio) was used for M1 macrophage staining and anti-Mannose receptor antibody (CD206, Abcam) was used for M2 macrophage staining [13]. Alexa Fluor® 594-AffiniPure Donkey Anti-Mouse IgG and Alexa Fluor® 488-AffiniPure Donkey Anti-Rabbit IgG (Jackson Immunoresearch) were used as secondary antibodies. DAPI mounting medium (Life Technologies) was applied to the slides. Images were taken using Zeiss Imager.A2 microscope using its Zen® interface.

To confirm specific staining for each primary antibody, an isotype control was used. For neutrophil staining, spleen sections were used as positive controls. All analysis was performed blinded by two observers. For H&E staining and CD31 IHC analysis, an arbitrary scale of 1–5 was used to grade the extent and intensity of chromogen present: 1: absence of staining; 2: faint scattered staining; 3: moderate staining; 4: intense staining; 5: very intense staining. Protein expression was measured in sham subcutaneous pockets and each of the scaffold embedded skin sections at both euthanasia time points. Qualitative comparison in protein expression is presented as a fold change for the scaffold skin compared to sham skin expression within the same rat. For macrophage IHC analysis, dual-stained cells were counted per visual field and data are presented as number of cells/field. At least 4 rats were used for all histological assays.

2.15. PCR array

Tissues from Sham, HEMA, 10/90, and 30/70 samples were snap frozen in liquid nitrogen and stored at −80 °C until processing. Total RNA was isolated using the RNase Microarray Tissue kit (Qiagen) according to the manufacturer's protocol. Yield and purity were quantified using a SpectraMax Plus 384 spectrophotometer (Molecular Devices). cDNA was prepared using 1 μg RNA with the RT^2 First Strand kit (Qiagen). Real-time PCR (RT-PCR) was performed on a Rat Wound Healing RT^2 Profiler PCR Array (SABiosciences). Ribosomal protein L13A (Rpl13a) and Lactase dehydrogenase A (Ldna) were used as housekeeping genes.

3. Results and discussion

3.1. pH-responsive scaffold fabrication and characterization

pH-responsive scaffolds were fabricated from the pH-sensitive monomer DMAEMA and biocompatible monomer HEMA via photopolymerization at predetermined molar ratios (10/90, 20/80, or 30/70, mol/mol) (Supplementary Fig. S1). A highly uniform porosity was achieved via particulate leaching of PMMA microparticles [14]. HEMA scaffolds were used as the non-responsive control.

Optical images of HEMA and DMAEMA/HEMA scaffolds are shown in Fig. 1a. Images of DMAEMA/HEMA scaffolds were also taken by bright field microscopy to observe swelling induced changes in pore size (Supplementary Fig. S2). The pore size of the 30/70 scaffold nearly doubled after swelling at pH 6.5 when compared to the initial non-swollen state. Scanning electron micrographs (SEM) of HEMA and 30/70 scaffolds demonstrated three-dimensional, interconnected pore structures (Fig. 1b and c).

Scaffold swelling was measured as a function of composition and pH (Fig. 1d–e, Supplementary Fig. S3a-d). The mass swelling ratio increased with the density of protonated amine groups in DMAEMA. The 30/70 scaffold expanded by 80% relative to HEMA at pH 5.5. Water is convected into DMAEMA/HEMA scaffolds to minimize electrostatic repulsion between cationic amines. Scaffold swelling was partially reversible, the 30/70 scaffold decreased by 40% (Supplementary Fig. S3e). We chose a physiological pH range

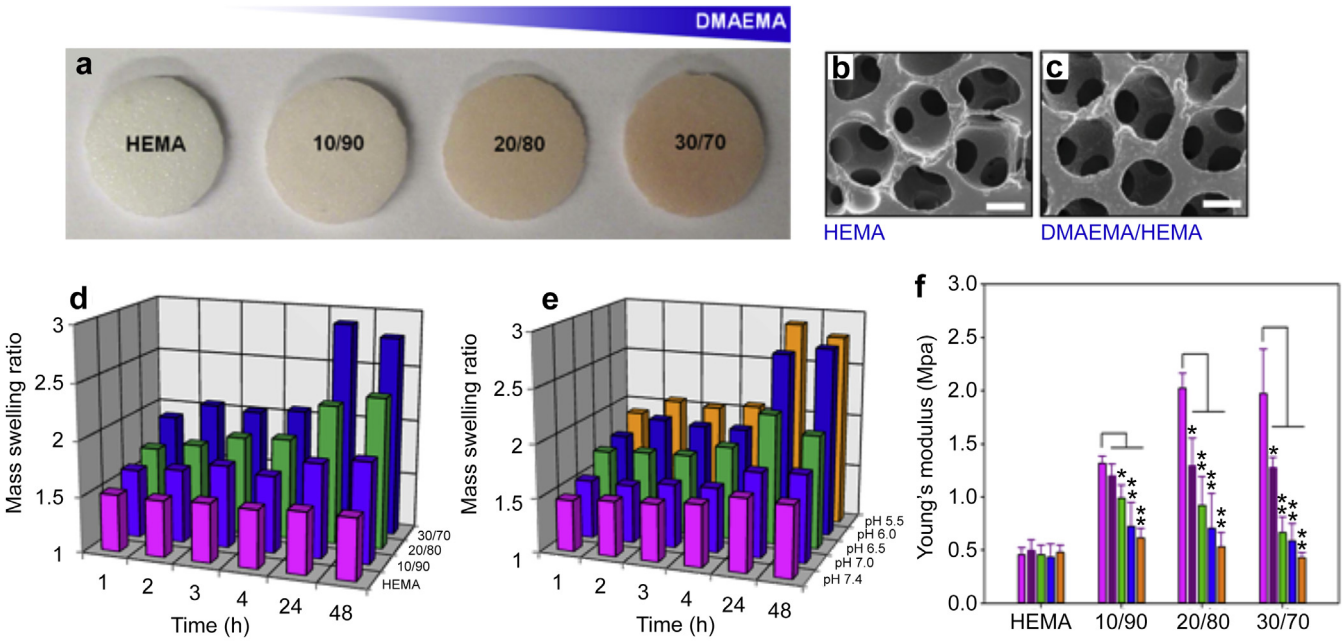

Fig. 1. Scaffold characterization. Optical micrograph images of (a) HEMA and pH-sensitive DMAEMA/HEMA scaffolds. Scale bar = 3 mm. SEM images of (b) Non-pH sensitive HEMA scaffold and (c) pH-sensitive DMAEMA/HEMA (30/70, mol/mol) scaffold. (d) Mass swelling ratio of HEMA (red) and pH-sensitive DMAEMA/HEMA scaffolds at different molar ratios (10/90 (purple), 20/80 (green), and 30/70 (blue), mol/mol) in pH 5.5 buffer as a function of time. (e) Mass swelling ratios of DMAEMA/HEMA scaffolds (30/70, mol/mol) in pH 5.5 (orange), 6.0 (blue), 6.5 (green), 7.0 (purple), and 7.4 (red) phosphate buffers. (f) Young's moduli of HEMA and pH-sensitive DMAEMA/HEMA scaffolds obtained after a 3 d incubation in pH 7.4 (red), 7.0 (purple), 6.5 (green), 6.0 (blue), and 5.5 (orange) buffer. The error is the standard deviation of the mean, where $n = 5$. Statistical significance was calculated using an unpaired t-test with $^{*}p < 0.05$. (For interpretation of the references to color in this figure legend, the reader is referred to the web version of this article.)

from 5.5 to 7.4; it is known that the extracellular pH can decrease to 6.5 in wound healing and 5.8 in tumor necrosis [15,16].

Swelling may stretch polymer chains, which can alter end-to-end distances of individual chains and therefore the bulk elasticity of the network [17]. Tensile tests were performed on scaffolds swollen from pH 5.5 to 7.4. As shown in Fig. 1f, the Young's moduli of DMAEMA/HEMA scaffolds were higher than HEMA at pH 7.4 but were comparable at pH 5.5. The Young's moduli of HEMA and 30/70 scaffolds at pH 7.4 were 0.46 ± 0.07 and 1.97 ± 0.42 MPa, respectively. At pH 5.5, the Young's moduli of 30/70 scaffold dropped to 0.43 ± 0.05 MPa. There was no significant difference in the elasticity of HEMA scaffolds between pH 5.5 and 7.4. Cells grown on substrates with Young's moduli between 0.6 and 2.6 MPa exhibited no differences in cell growth [18].

3.2. Cellular response and oxygen dynamics

Fibronectin-coated scaffolds were seeded with NIH/3T3 mouse fibroblasts (1.0×10^6 and 1.0×10^7 cells/mL) and evaluated for changes in pH and oxygen content (pO_2). A fibronectin coating was used to minimize differences in scaffold composition. The pH of the growth media decreased after 72 h for both cell densities (Fig. 2a). Similarly, the oxygen level decreased at the center of the scaffold as time progressed (Fig. 2b). The 10/90 scaffold had less oxygen than the 20/80 and 30/70 scaffolds; HEMA scaffolds had the lowest pO_2 values. Fig. 2c and d show fluorescence micrographs of cells after 3 d of culture on HEMA and 30/70 scaffolds, respectively. Cells homogeneously grew throughout the responsive scaffolds but were clustered on the HEMA scaffold. This was consistent with the increase in cell number over a 3 d period on the responsive scaffolds (Fig. 2e). In contrast, the number of cells declined on HEMA scaffolds over the same period.

Molecular oxygen is essential for intracellular processes; biosynthesis, migration, and transport require energy supplied by the coenzyme adenosine-triphosphate (ATP), which is synthesized by mitochondrial oxidative phosphorylation [19]. During the inflammatory phase of wound healing, NADPH-linked oxygenase produces oxidants by consuming high amounts of oxygen, which are needed to prevent infection [20]. Oxygen is also needed for collagen synthesis; the hydroxylation of proline and lysine in procollagen is necessary to form stable triple helices [21]. Thus, successful wound healing can only occur in the presence oxygen, which is more readily available within the pH-responsive scaffolds.

In an effort to distinguish the contribution from oxygen and scaffold stretching, cells were grown on PLG, HEMA, 10/90 and 30/70 scaffolds under hypoxic conditions (Fig. 2f). We included PLG in this study as it is widely used in tissue engineering; it does not swell in response to pH but can degrade by hydrolysis [22]. The HEMA and DMAEMA/HEMA scaffold compositions are non-degradable over the course of our study. At day 3, no significant differences were observed between the 30/70 and HEMA scaffolds; PLG scaffolds, however, suffered a decline in number of cells. The increased oxygen availability of 30/70 scaffolds cultured at 21% O_2 accounted for a 30% increase in cell number on day 3 relative to the HEMA (Fig. 2e). By day 7, the 30/70 scaffold demonstrated a 48% and 76% increase in cell number compared to HEMA and PLG under hypoxia, respectively. Cyclic or constant tensile strain can induce cell signal transduction *in vitro* [23] and *in vivo* [24], respectively. Thus, scaffold stretching was able to induce cell growth at low oxygen conditions.

3.3. Modeling oxygen concentration in stretched scaffolds

To further evaluate oxygen availability in our scaffolds as a function of swelling, we developed a finite element model simulating the oxygen concentration as a function of distance from the center to the exterior of the scaffold. The time-dependent oxygen concentration is equal to the diffusion of oxygen into the scaffold minus the rate of consumption:

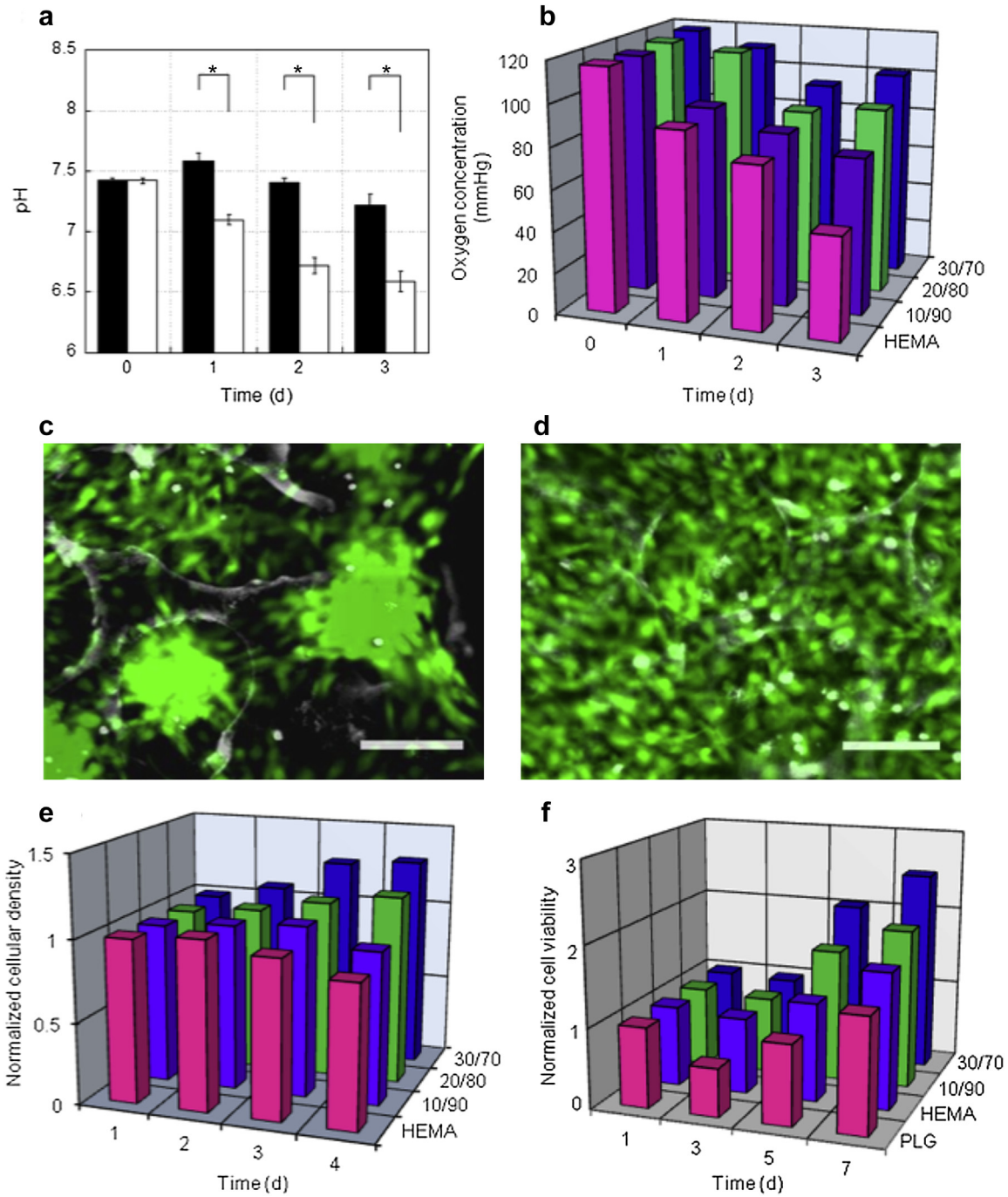

Fig. 2. Changes in pH, oxygen concentration, and cell density. (a) pH measurements of the growth medium for 30/70 (mol/mol) scaffolds seeded with NIH/3T3 cells at an initial density of 10^6 cells/scaffold (black bars) and 10^7 cells/scaffold (white bars). Statistical significance was calculated using an unpaired t-test with $^*p < 0.05$. (b) Oxygen concentration at the center of HEMA (red) and pH-sensitive DMAEMA/HEMA (10/90 (purple), 20/80 (green), and 30/70 (blue), mol/mol) scaffolds seeded with NIH/3T3 cells as a function of time. Fluorescent micrographs of NIH/3T3 cells seeded on (c) HEMA and (d) pH-sensitive DMAEMA/HEMA scaffolds after 72 h, stained with the Live/Dead assay. Scale bar = 100 μm. (e) Normalized cell density of NIH/3T3 cells on HEMA (red) and pH-sensitive DMAEMA/HEMA (10/90 (purple), 20/80 (green), and 30/70 (blue), mol/mol) scaffolds as a function of time. (f) Normalized cell density of NIH/3T3 cells on HEMA (red), PLG (purple), and pH-sensitive DMAEMA/HEMA (10/90 (green), and 30/70 (blue), mol/mol) scaffolds as a function of time under hypoxic conditions (5% O_2. 10^7 NIH/3T3 cells were seeded initially (b–f)). (For interpretation of the references to color in this figure legend, the reader is referred to the web version of this article.)

$$\frac{\partial C(r,t)}{\partial t} = D\left(\frac{\partial^2 C(r,t)}{\partial r^2} + \frac{1}{r}\frac{\partial C}{\partial r}\right) - \beta\rho(t) \qquad (1)$$

where C(r,t) is the oxygen concentration, t is time, D is the diffusion coefficient of oxygen in tissue, r is the radius of the scaffold, β is the oxygen consumption rate per cell, ρ is the cell density, h is the scaffold width, and λ(t) is the uniform scaffold stretch. The scaffold stretch λ is described by $\lambda(t) = r(t)/r_0$. Thus, r_0 is a moving boundary that allows the scaffold to grow into the surrounding medium. The swelling of the hydrogel (Fig. 3a), which was fit to experimental observations (Fig. 1e), is described by the following equation:

$$\lambda(t) = 1 + \left(\lambda_f - 1\right)\left(1 - e^{-0.11t}\right) \quad (2)$$

where t is in hours. The cell density is dependent on the volume; it decreases as the scaffold swells. The cell density is then defined:

$$\rho(t) = \frac{n}{\pi(r^*\lambda(t))^2 h} \quad (3)$$

If we set the initial oxygen concentration throughout the scaffold equal to the external medium, the flux at the center of the scaffold equal to zero, and the oxygen concentration at the periphery constant due to mixing, then the oxygen concentration at the center of the scaffold will decrease as time progresses. In the absence of cell proliferation, the oxygen profile will reach a balance between oxygen diffusing in and oxygen being consumed. A necrotic region is then defined by a distance from the center of the scaffold where the oxygen concentration cannot support cell growth. For non-responsive scaffolds ($\lambda_f = 1$), the necrotic region increased from 0.06 to 0.40 cm as the half-width increased from 0.40 to 0.72 cm (Fig. 3c–d). In contrast, growth of the necrotic region was halted (at x = 0.10 cm) as the 30/70 scaffold ($\lambda_f = 1.8$) expanded from 0.4 to 0.72 cm (Fig. 3b). The area of the necrotic region is 1600% larger in the non-responsive scaffold relative to the pH-responsive scaffold. This substantial change in the oxygen profile across the 30/70 scaffold is in part responsible for the increased cell viability.

3.4. Determining the biological response of pH-sensing scaffolds in vivo

Responsive scaffolds were implanted subcutaneously in rats for a period of 7 and 14 d. This initial animal model was chosen to demonstrate differences in cell infiltration, neovascularization, and immune response. Qualitatively, pH-responsive scaffolds visualized after explantation showed the highest level of cell infiltration (Supplementary Fig. S4). As seen in the sham wounds, little to no inflammation and tissue remodeling was observed. We observed a significant increase in granulation tissue after 7 and 14 d in the 30/70 scaffold relative to Sham (Fig. 4a,c, Supplementary Fig. S5). An increased cellular in-growth into scaffolds was anticipated given

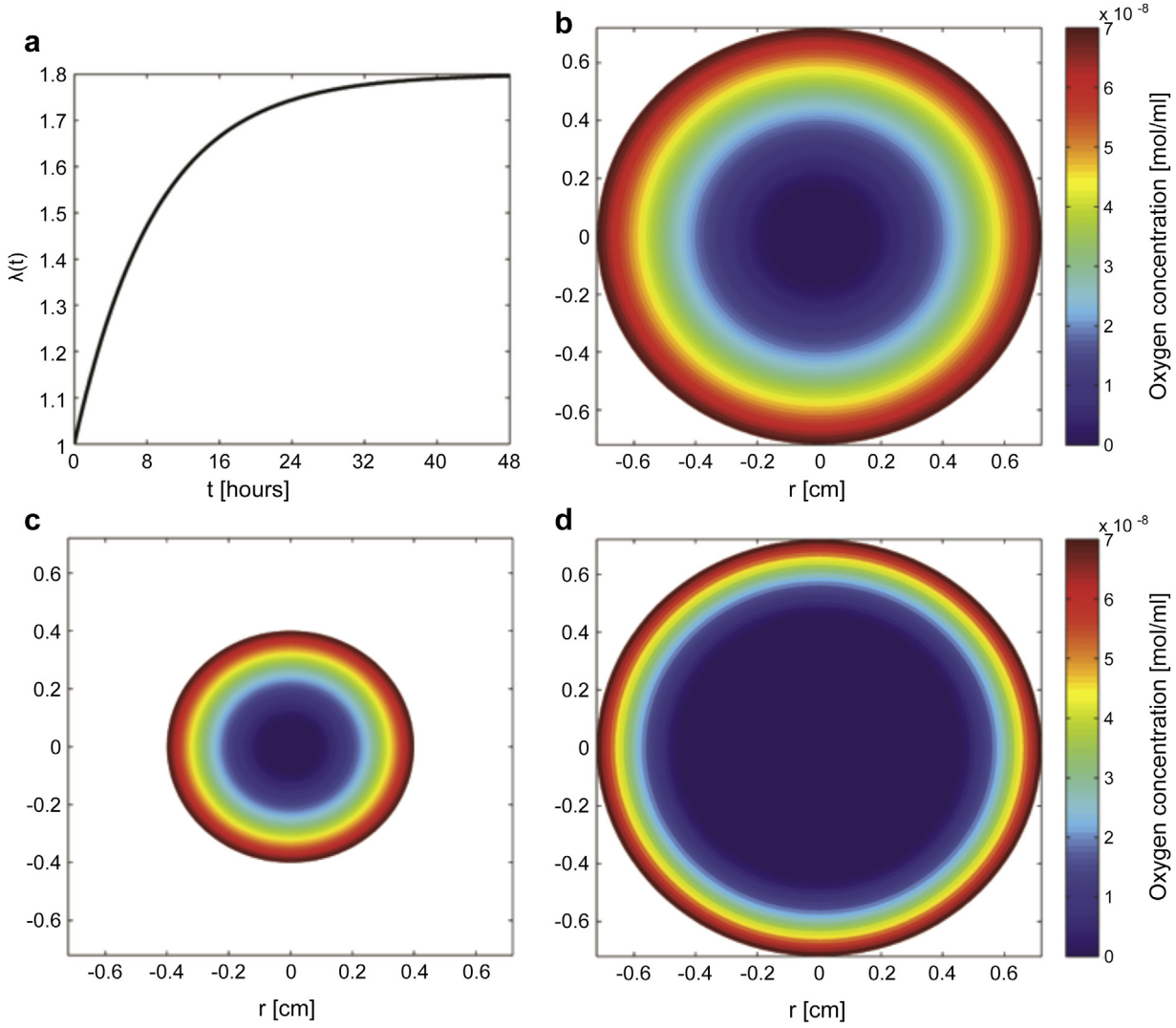

Fig. 3. Mathematical model of scaffold oxygen concentration. (a) Scaffold swelling as a function of time (λ) approximated given data for 30/70 scaffold, (b) Oxygen concentration after 48 h in a responsive scaffold that swells from r = 0.4 cm–0.72 cm (λ = 1.8, similar to 30/70 DMAEMA/HEMA scaffold). (c) and (d) show the oxygen concentration for a non-responsive scaffold (λ = 1) with radius (c) r_0 = 0.4 cm and (d) r_0 = 0.72 cm. The color legend (b–d) indicates the oxygen concentration; the dark blue region is necrotic. (For interpretation of the references to color in this figure legend, the reader is referred to the web version of this article.)

the superior oxygen permeability and mechanical stretching of 30/70 scaffolds. In fact, all 30/70 scaffolds elicited profound tissue formation largely in the absence of significant wounding. Implanted scaffolds were also assessed for vascularization by immunostaining for cluster of differentiation 31 (CD31), present in endothelial cell intercellular junctions (Fig. 4b, Supplementary Fig. S7). The 10/90 and 30/70 conditions exhibited the highest expression of CD31 after implantation; however, these differences were not pronounced (Fig. 4d). Angiogenesis may be induced by both hypoxic [25] and mechanical cues [23]. These observations not only support the present *in vitro* data of cellular scaffold infiltration but are highly promising for a future application in poorly granulating, anergic wound beds.

To further characterize infiltrating cells, tissues were immunostained for macrophages (Fig. 5a) and neutrophils (Supplementary Fig. S6). Macrophage subtype staining revealed a trend towards a higher presence of M1 (the pro-inflammatory phenotype) and M2 macrophages (the pro-healing phenotype) in 10/90 and 30/70 scaffolds compared to HEMA (Fig. 5b). The moderate macrophage response was expected as only a minor tissue injury occurred during blunt dissection at the site of scaffold implantation. The M1/M2 ratio did not differ between treatment groups; an increased

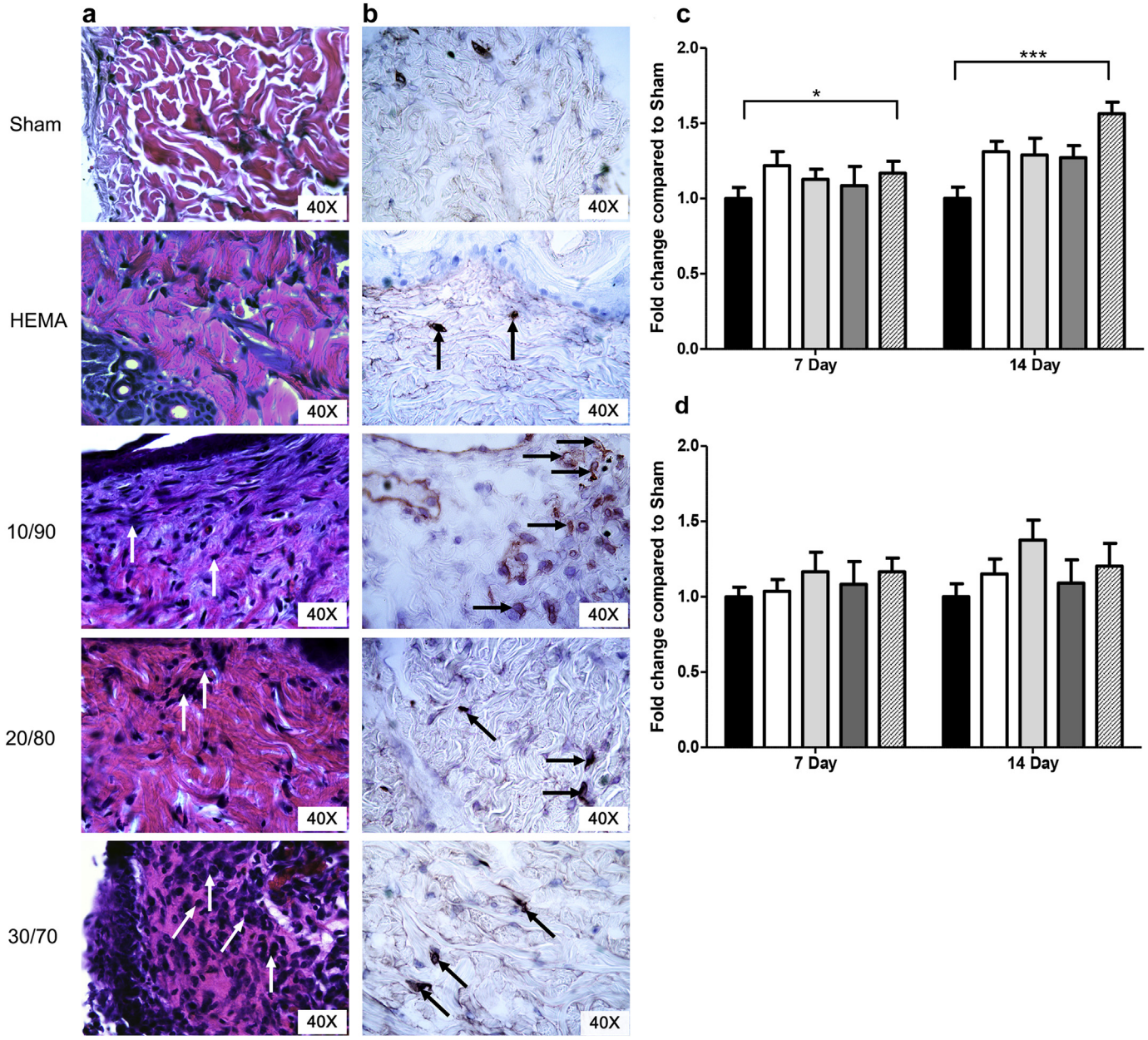

Fig. 4. Cell infiltration quantification. (a) Hematoxylin and eosin (H&E) stained sections were analyzed. Representative images close to scaffold implantation for Sham, HEMA, 10/90, 20/80, and 30/70 groups after 14 d (Mag = 40×). Arrows indicate cell infiltration. (b) CD31 immunostained sections were analyzed for vascularization. Representative positive staining images of Sham, HEMA, 10/90, 20/80, and 30/70 groups after 14 d (Mag = 40×). Arrows indicate staining of endothelial cells. Scoring of the H&E stained sections after (c) 7 and 14 d. Scoring of the CD31 immunostained sections after (d) 7 and 14 d. All scores were normalized to the Sham condition. Black, white, light grey, dark grey, and striped bars correspond to Sham, HEMA, 10/90, 20/80, and 30/70 conditions, respectively. Error bars shown are reported as standard error. Statistical significance was calculated using 2-way ANOVA analysis with $^{*}p < 0.05$ and $^{***}p < 0.001$. A statistically significant difference in score was also found between the Sham and HEMA condition at 7 and 14 d for the H&E analysis.

M1/M2 ratio is a hallmark of abnormal wound healing (Fig. 5c). As expected by day 14, neutrophils were absent in all groups. To confirm the absence of neutrophils, we used a rat spleen section as a positive control.

3.5. Genetic profiling of scaffold-tissue interactions

The effect of scaffold implantation on gene expression was evaluated using a Rat Wound Healing PCR Array. The regulation of inflammatory cytokines, growth factors, cell adhesion markers, extracellular matrix (ECM) and signal transduction molecules was examined (Supplementary Fig. S8–S13, Supplementary Table S1–S3). We observed that genes were often upregulated in the 30/70 scaffold relative to Sham and HEMA; data were adjusted to highlight statistically significant changes compared to the Sham group ($p < 0.05$) (Fig. 6a, Supplementary Fig. S14).

In the present study, chemokine (C-X-C motif) ligand 3 (CXCL3) and Tumor Necrosis Factor alpha (TNFα) were significantly increased in the 30/70 scaffold relative to HEMA (Fig. 6b and c). CXCL3 regulates angiogenesis via the recruitment and adhesion of leukocytes [26]. The role of TNFα is controversial in wound healing and depends on concentration, length of exposure, and presence of other cytokines [27]. TNFα is linked to increased collagen production whereas in other reports it is implicated in non-healing wounds [27]. In contrast, CD40 ligand (CD40l) was significantly increased in HEMA and 10/90 scaffolds but not in 30/70 scaffolds (Fig. 6d). CD40l, a member of the TNF family, leads to inflammation [28], endothelial dysfunction [29], neointimal formation after vascular injury [30] and ischemia-reperfusion tissue injury [31]. Significant changes in cytokine regulation that support wound healing were therefore observed in 30/70 scaffolds relative to HEMA.

Other cytokines, such as Interleukin-6 (IL6), were upregulated in responsive scaffolds compared to Sham whereas no statistical significance was observed between HEMA and Sham (Fig. 6e). IL6 is credited with regulating leukocyte infiltration, angiogenesis, and collagen accumulation [32]. Knockout and/or antibody blocking of IL6 reduced wound healing in mice [32]. An acute increase in inflammatory cytokines after injury is the first-step towards normal wound healing. Chronic inflammation, as observed in diabetes, can

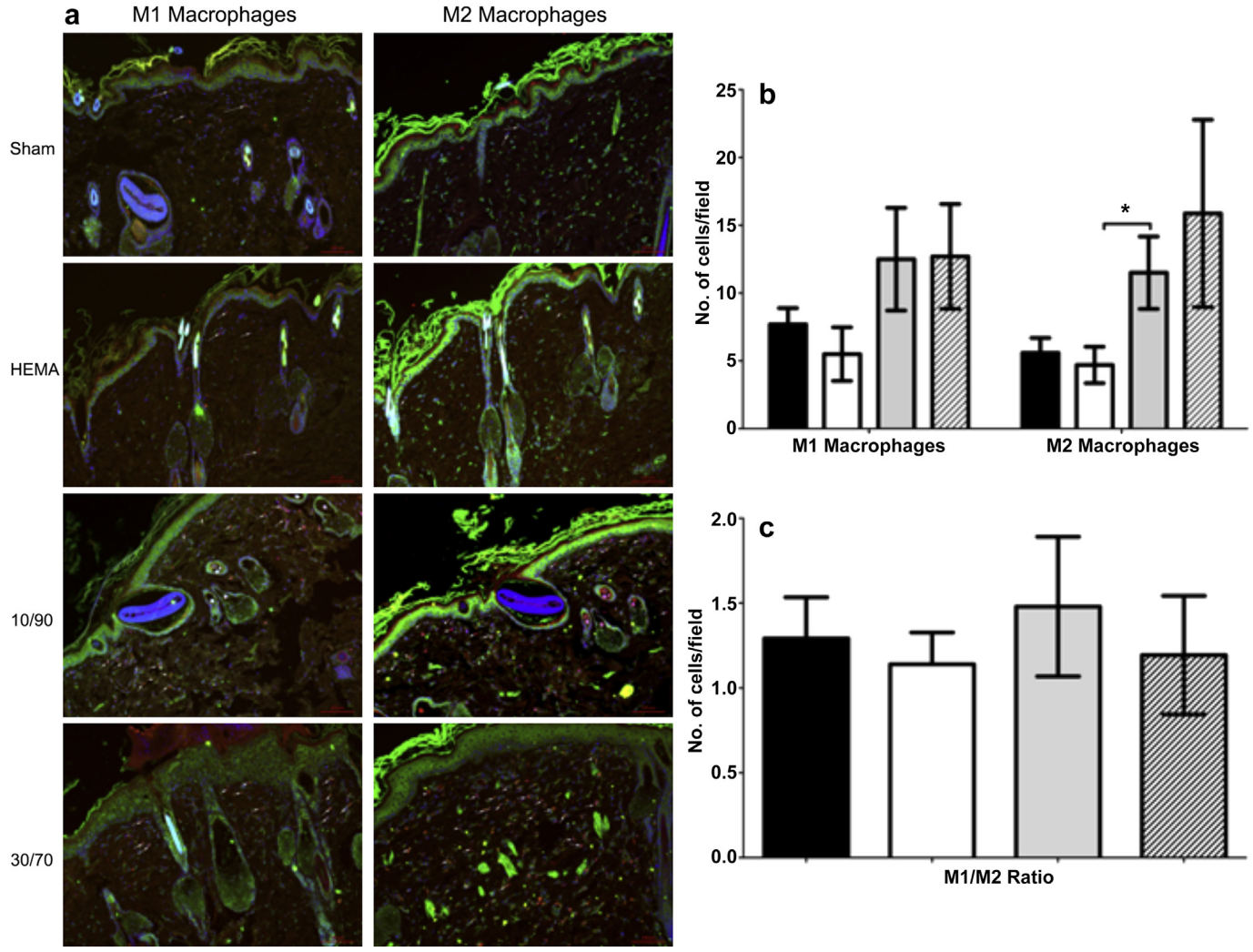

Fig. 5. Macrophage infiltration. (a) Formalin fixed paraffin embedded 6 μm cross-sections were analyzed for macrophage infiltration. CD-68 was used as a pan-macrophage marker, TNFα was used for M1 specific macrophage staining and anti-CD206 was used for M2 specific macrophage staining. Representative positive dual stained images of Sham, HEMA, 10/90, and 30/70 groups after 14 d. Orange-yellow stains indicate dual-stained macrophages. (b) Scoring of the M1 and M2 macrophage immunostained sections after 14 d (c) M1/M2 ratio based on scoring in (b). Dual stained cells were counted per field of view. Black, white, light grey, and striped bars correspond to Sham, HEMA, 10/90, and 30/70 conditions, respectively. Error bars shown are reported as standard error. Statistical significance was calculated using 1-way ANOVA analysis and unpaired t-test with *$p < 0.05$. (For interpretation of the references to color in this figure legend, the reader is referred to the web version of this article.)

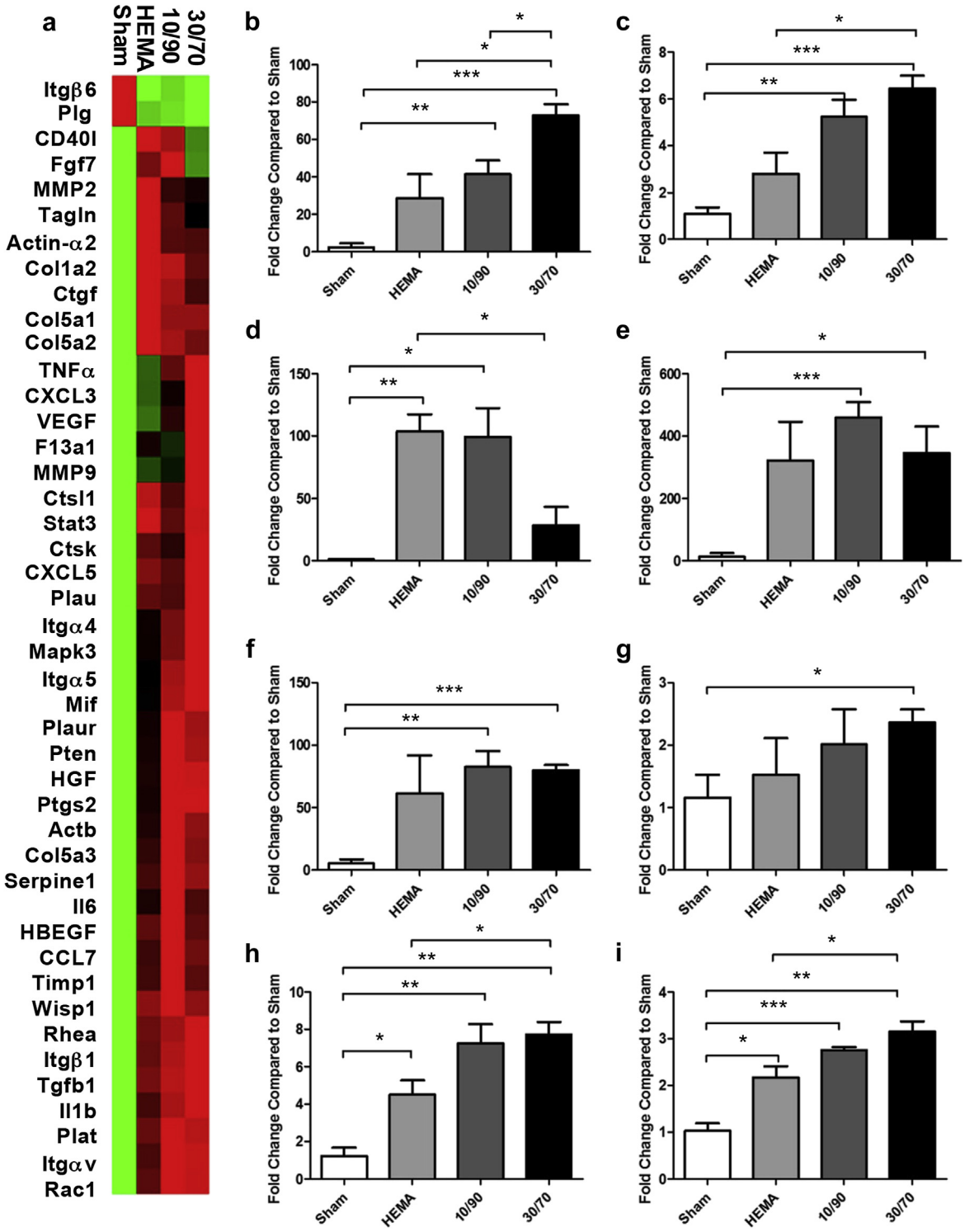

Fig. 6. Wound healing gene profile. (a) Gene expression analysis of tissue samples near implanted scaffolds *in vivo*. Red and green represent maximum and minimum gene expression, respectively. Supplementary Table S3 defines abbreviations. Normalized gene expression analysis of (b) CXCL3, (c) TNFα, (d) CD40l, (e) IL6, (f) HGF, (g) VEGF, (h) Itg α5, and (i) MAPK3. All error bars represent standard error, where $n = 3$. Statistical significance was calculated using a Student's t-test of the replicate 2^{-}(-dCt) values for each gene in the Sham group and treatment groups with $^{*}p < 0.05$, $^{**}p < 0.01$, and $^{***}p < 0.001$. (For interpretation of the references to color in this figure legend, the reader is referred to the web version of this article.)

lead to an insufficient or dysregulated cytokine response during the inflammatory phase, which impairs wound healing [33,34]. Scaffolds that induce an acute cytokine response to injury may consequently promote wound healing.

In the growth factor category, hepatocyte growth factor (HGF), heparin binding epidermal growth factor (HBEGF), and vascular endothelial growth factor (VEGF) were significantly increased in the 30/70 scaffolds relative to Sham while no statistical difference

was observed between HEMA and Sham (Fig. 6f–g). These growth factors are essential for cutaneous wound healing and angiogenesis [35–37].

Integrins (Itg) are important cell adhesion molecules that form heterodimers and assist in cell–cell interactions and cell-ECM interactions thereby participating in all phases of wound healing from immune response to remodeling. Itg α5 was significantly higher in the 30/70 group compared to HEMA (Fig. 6h). Remodeling by integrins and cytoskeletal proteins have been reported to trigger leukocyte recruitment, fibroblast migration, proliferation, and angiogenesis [38–40]. Thus, the 30/70 scaffold may support wound healing by increasing cell adhesion and migration.

Mitogen-activated protein kinase 3 (MAPK3, a.k.a. ERK1), known to play an important role in the VEGF signaling pathway [41], is significantly increased in the 30/70 scaffold relative to HEMA (Fig. 6i). MAPK3 regulates cellular proliferation, differentiation, and cell cycle progression in response to cytokines or growth factor stimulation [42]. Of the cytoskeleton proteins, alpha smooth muscle actin (Actin-α2) and actin-β were significantly increased in 30/70 compared to Sham. This suggests high proliferative and/or synthetic activity of infiltrating smooth muscle and local cells.

Overall, the data suggest that the 30/70 scaffold leads to a pro-healing milieu of cytokines and growth factors, which induce signal transduction that results in significant granulocyte tissue formation and vascularization relative to HEMA. In contrast, the synthetic scaffold PLG is observed to have an inflammatory response resulting in the formation of a thick fibrous capsule by day 14 [43]. PLG does not support cell infiltration [44] or cell proliferation (Fig. 2f). The acidic byproducts present upon degradation may result in an unfavorable inflammatory response and cytotoxicity [45].

Of note, subcutaneous scaffold implantation in an uninjured healthy animal does not reflect the cellular responses in a chronic wound rather; it represents the body's response to the implanted material. As discussed above, responsive 30/70 scaffolds are superior to HEMA in host tissue immune response to scaffold implantation. Further, we provide compelling evidence that 30/70 scaffold implantation leads to formation of high amounts of granulating tissue, including macrophage infiltration. Inability to develop granulation tissue is a hallmark of impaired diabetic wounds [46]. Enzymatic or surgical debridement is often needed to stimulate healthy granulation tissue formation. Therefore, a scaffold such as the 30/70 with its high propensity for attracting leukocytes and forming granulation tissue is strongly desirable. Although the DMAEMA/HEMA scaffolds in this study were non-degradable, future preclinical and/or clinical applications can utilize crosslinkers that degrade by hydrolysis [47]. Local dysregulation of inflammatory signals and a local paucity of acute inflammatory response to injury is thought to be partially responsible for the poor healing response, particularly in diabetic wounds. The 30/70 scaffolds may prove to be dually beneficial as they induce a predominantly favorable cytokine inflammatory profile as well as significant mitogenic, angiogenic, and remodeling stimuli.

4. Conclusions

In summary, we have demonstrated that pH-sensitive scaffolds that swell in response to a decrease in pH encourage wound healing. Responsive DMAEMA/HEMA scaffolds exhibited increased granulation tissue *in vivo* and upregulated factors that promote tissue regeneration. To date, no scaffold has mimicked the pro-healing gene profile characteristic of mechanical manipulation due in part to the body's ability to rapidly equilibrate to stress. The stretch induced by the responsive scaffold may play a role in altering the gene expression profile observed in our results. Scaffolds that respond to environmental changes show potential for the improved treatment of chronic wounds.

Acknowledgments

This work was supported primarily by the MRSEC program of the National Science Foundation under award number DMR-0820484. This work was performed in part at the Center for Nanoscale Systems (CNS), a member of the National Nanotechnology Infrastructure Network (NNIN), which is supported by the National Science Foundation under NSF award no. ECS-0335765. CNS is part of the Faculty of Arts and Sciences at Harvard University. FWL and LPN were supported by the William J. von Liebig Foundation award.

Appendix A. Supplementary data

Supplementary data related to this article can be found at http://dx.doi.org/10.1016/j.biomaterials.2015.04.011.

References

[1] Sen CK, Gordillo GM, Roy S, Kirsner R, Lambert L, Hunt TK, et al. Human skin wounds: a major and snowballing threat to public health and the economy. Wound Repair Regen 2009;17:763–71.
[2] Sen CK. Wound healing essentials: let there be oxygen. Wound Repair Regen 2009;17:1–18.
[3] Zhong SP, Zhang YZ, Lim CT. Tissue scaffolds for skin wound healing and dermal reconstruction. Wiley Interdiscip Rev Nanomed Nanobiotechnol 2010;2:510–25.
[4] Levenberg S, Rouwkema J, Macdonald M, Garfein ES, Kohane DS, Darland DC, et al. Engineering vascularized skeletal muscle tissue. Nat Biotechnol 2005;23:879–84.
[5] Miller JS, Stevens KR, Yang MT, Baker BM, Nguyen DH, Cohen DM, et al. Rapid casting of patterned vascular networks for perfusable engineered three-dimensional tissues. Nat Mater 2012;11:768–74.
[6] Leong MF, Toh JK, Du C, Narayanan K, Lu HF, Lim TC, et al. Patterned prevascularised tissue constructs by assembly of polyelectrolyte hydrogel fibres. Nat Commun 2013;4:2353.
[7] Lemasters JJ, Nieminen AL, Qian T, Trost LC, Elmore SP, Nishimura Y, et al. The mitochondrial permeability transition in cell death: a common mechanism in necrosis, apoptosis and autophagy. Biochim Biophys Acta 1998;1366:177–96.
[8] Schumpp B, Schlaeger EJ. Optimization of culture conditions for high cell density proliferation of HL-60 human promyelocytic leukemia cells. J Cell Sci 1990;97(Pt 4):639–47.
[9] van de Wetering P, Moret EE, Schuurmans-Nieuwenbroek NM, van Steenbergen MJ, Hennink WE. Structure-activity relationships of water-soluble cationic methacrylate/methacrylamide polymers for nonviral gene delivery. Bioconjug Chem 1999;10:589–97.
[10] You JO, Auguste DT. Nanocarrier cross-linking density and pH sensitivity regulate intracellular gene transfer. Nano Lett 2009;9:4467–73.
[11] Synatschke CV, Schallon A, Jerome V, Freitag R, Muller AH. Influence of polymer architecture and molecular weight of poly(2-(dimethylamino)ethyl methacrylate) polycations on transfection efficiency and cell viability in gene delivery. Biomacromolecules 2011;12:4247–55.
[12] Muschler GF, Nakamoto C, Griffith LG. Engineering principles of clinical cell-based tissue engineering. J Bone Jt Surg Am 2004;86-A:1541–58.
[13] Biswas SK, Mantovani A. Macrophage plasticity and interaction with lymphocyte subsets: cancer as a paradigm. Nat Immunol 2010;11:889–96.
[14] You JO, Rafat M, Ye GJ, Auguste DT. Nanoengineering the heart: conductive scaffolds enhance connexin 43 expression. Nano Lett 2011;11:3643–8.
[15] Woo YC, Park SS, Subieta AR, Brennan TJ. Changes in tissue pH and temperature after incision indicate acidosis may contribute to postoperative pain. Anesthesiology 2004;101:468–75.
[16] Tannock IF, Rotin D. Acid pH in tumors and its potential for therapeutic exploitation. Cancer Res 1989;49:4373–84.
[17] Patel A, Mequanint K. Hydrogel biomaterials. In: Fazel-Rezai R, editor. Biomedical engineering - frontiers and challenges; 2011.
[18] Lee JN, Jiang X, Ryan D, Whitesides GM. Compatibility of mammalian cells on surfaces of poly(dimethylsiloxane). Langmuir 2004;20:11684–91.
[19] Mitchell P. Coupling of phosphorylation to electron and hydrogen transfer by a chemi-osmotic type of mechanism. Nature 1961;191:144–8.
[20] Allen DB, Maguire JJ, Mahdavian M, Wicke C, Marcocci L, Scheuenstuhl H, et al. Wound hypoxia and acidosis limit neutrophil bacterial killing mechanisms. Arch Surg 1997;132:991–6.
[21] Hunt TK, Zederfeldt B, Goldstick TK. Oxygen and healing. Am J Surg 1969;118:521–5.

[22] Thomson RC, Wake MC, Yaszemski MJ, Mikos AG. Biodegradable polymer scaffolds to regenerate organs. Adv Polym Sci 1995;122:245–74.
[23] Yung YC, Chae J, Buehler MJ, Hunter CP, Mooney DJ. Cyclic tensile strain triggers a sequence of autocrine and paracrine signaling to regulate angiogenic sprouting in human vascular cells. Proc Natl Acad Sci U S A 2009;106:15279–84.
[24] Morykwas MJ, Argenta LC, Shelton-Brown EI, McGuirt W. Vacuum-assisted closure: a new method for wound control and treatment: animal studies and basic foundation. Ann Plast Surg 1997;38:553–62.
[25] Pugh CW, Ratcliffe PJ. Regulation of angiogenesis by hypoxia: role of the HIF system. Nat Med 2003;9:677–84.
[26] Strieter RM, Burdick MD, Gomperts BN, Belperio JA, Keane MP. CXC chemokines in angiogenesis. Cytokine Growth Factor Rev 2005;16:593–609.
[27] Roy S, Dickerson R, Khanna S, Collard E, Gnyawali U, Gordillo GM, et al. Particulate beta-glucan induces TNF-alpha production in wound macrophages via a redox-sensitive NF-kappabeta-dependent pathway. Wound Repair Regen 2011;19:411–9.
[28] Dormond O, Contreras AG, Meijer E, Datta D, Flynn E, Pal S, et al. CD40-induced signaling in human endothelial cells results in mTORC2- and Akt-dependent expression of vascular endothelial growth factor in vitro and in vivo. J Immunol 2008;181:8088–95.
[29] Hristov M, Gumbel D, Lutgens E, Zernecke A, Weber C. Soluble CD40 ligand impairs the function of peripheral blood angiogenic outgrowth cells and increases neointimal formation after arterial injury. Circulation 2010;121:315–24.
[30] Song Z, Jin R, Yu S, Nanda A, Granger DN, Li G. Crucial role of CD40 signaling in vascular wall cells in neointimal formation and vascular remodeling after vascular interventions. Arterioscler Thromb Vasc Biol 2012;32:50–64.
[31] Bhogal RH, Weston CJ, Curbishley SM, Adams DH, Afford SC. Activation of CD40 with platelet derived CD154 promotes reactive oxygen species dependent death of human hepatocytes during hypoxia and reoxygenation. PLoS One 2012;7:e30867.
[32] Lin ZQ, Kondo T, Ishida Y, Takayasu T, Mukaida N. Essential involvement of IL-6 in the skin wound-healing process as evidenced by delayed wound healing in IL-6-deficient mice. J Leukoc Biol 2003;73:713–21.
[33] Pradhan L, Cai X, Wu S, Andersen ND, Martin M, Malek J, et al. Gene expression of pro-inflammatory cytokines and neuropeptides in diabetic wound healing. J Surg Res 2011;167:336–42.
[34] Pradhan L, Nabzdyk C, Andersen ND, LoGerfo FW, Veves A. Inflammation and neuropeptides: the connection in diabetic wound healing. Expert Rev Mol Med 2009;11:e2.
[35] Serrano I, Diez-Marques ML, Rodriguez-Puyol M, Herrero-Fresneda I, Raimundo Garcia del M, Dedhar S, et al. Integrin-linked kinase (ILK) modulates wound healing through regulation of hepatocyte growth factor (HGF). Exp Cell Res 2012;318:2470–81.
[36] Stoll SW, Rittie L, Johnson JL, Elder JT. Heparin-binding EGF-like growth factor promotes epithelial-mesenchymal transition in human keratinocytes. J Invest Dermatol 2012;132:2148–57.
[37] Rico T, Green J, Kirsner RS. Vascular endothelial growth factor delivery via gene therapy for diabetic wounds: first steps. J Invest Dermatol 2009;129:2084.
[38] Shyy JY, Chien S. Role of integrins in cellular responses to mechanical stress and adhesion. Curr Opin Cell Biol 1997;9:707–13.
[39] Rose DM, Alon R, Ginsberg MH. Integrin modulation and signaling in leukocyte adhesion and migration. Immunol Rev 2007;218:126–34.
[40] Larsen M, Artym VV, Green JA, Yamada KM. The matrix reorganized: extracellular matrix remodeling and integrin signaling. Curr Opin Cell Biol 2006;18:463–71.
[41] Andrikopoulos P, Baba A, Matsuda T, Djamgoz MB, Yaqoob MM, Eccles SA. Ca2+ influx through reverse mode Na+/Ca2+ exchange is critical for vascular endothelial growth factor-mediated extracellular signal-regulated kinase (ERK) 1/2 activation and angiogenic functions of human endothelial cells. J Biol Chem 2011;286:37919–31.
[42] Matsubayashi Y, Ebisuya M, Honjoh S, Nishida E. ERK activation propagates in epithelial cell sheets and regulates their migration during wound healing. Curr Biol 2004;14:731–5.
[43] Wang Y, Ameer GA, Sheppard BJ, Langer R. A tough biodegradable elastomer. Nat Biotechnol 2002;20:602–6.
[44] Kim MS, Ahn HH, Shin YN, Cho MH, Khang G, Lee HB. An in vivo study of the host tissue response to subcutaneous implantation of PLGA- and/or porcine small intestinal submucosa-based scaffolds. Biomaterials 2007;28:5137–43.
[45] Shive MS, Anderson JM. Biodegradation and biocompatibility of PLA and PLGA microspheres. Adv Drug Deliv Rev 1997;28:5–24.
[46] Blakytny R, Jude E. The molecular biology of chronic wounds and delayed healing in diabetes. Diabet Med 2006;23:594–608.
[47] Bryant SJ, Cuy JL, Hauch KD, Ratner BD. Photo-patterning of porous hydrogels for tissue engineering. Biomaterials 2007;28:2978–86.